Biases in the air-sea flux of CO_2 resulting from ocean surface temperature gradients

B. Ward,[1] R. Wanninkhof,[2] W. R. McGillis,[1] A. T. Jessup,[3] M. D. DeGrandpre,[4] J. E. Hare,[5] and J. B. Edson[1]

Received 28 January 2003; revised 5 August 2003; accepted 7 November 2003; published 30 June 2004.

[1] The difference in the fugacities of CO_2 across the diffusive sublayer at the ocean surface is the driving force behind the air-sea flux of CO_2. Bulk seawater fugacity is normally measured several meters below the surface, while the fugacity at the water surface, assumed to be in equilibrium with the atmosphere, is measured several meters above the surface. Implied in these measurements is that the fugacity values are the same as those across the diffusive boundary layer. However, temperature gradients exist at the interface due to molecular transfer processes, resulting in a cool surface temperature, known as the skin effect. A warm layer from solar radiation can also result in a heterogeneous temperature profile within the upper few meters of the ocean. Here we describe measurements carried out during a 14-day study in the equatorial Pacific Ocean (GasEx-2001) aimed at estimating the gradients of CO_2 near the surface and resulting flux anomalies. The fugacity measurements were corrected for temperature effects using data from the ship's thermosalinograph, a high-resolution profiler (SkinDeEP), an infrared radiometer (CIRIMS), and several point measurements at different depths on various platforms. Results from SkinDeEP show that the largest cool skin and warm layer biases occur at low winds, with maximum biases of −4% and +4%, respectively. Time series ship data show an average CO_2 flux cool skin retardation of about 2%. Ship and drifter data show significant CO_2 flux enhancement due to the warm layer, with maximums occurring in the afternoon. Temperature measurements were compared to predictions based on available cool skin parameterizations to predict the skin-bulk temperature difference, along with a warm layer model. *INDEX TERMS:* 0312 Atmospheric Composition and Structure: Air/sea constituent fluxes (3339, 4504); 4594 Oceanography: Physical: Instruments and techniques; 4820 Oceanography: Biological and Chemical: Gases; 1635 Global Change: Oceans (4203); *KEYWORDS:* air-sea CO_2 flux, warm layer, cool skin

Citation: Ward, B., R. Wanninkhof, W. R. McGillis, A. T. Jessup, M. D. DeGrandpre, J. E. Hare, and J. B. Edson (2004), Biases in the air-sea flux of CO_2 resulting from ocean surface temperature gradients, *J. Geophys. Res.*, *109*, C08S08, doi:10.1029/2003JC001800.

1. Introduction

[2] Our understanding of global oceanic uptake of CO_2 is partly derived from a combination of measurements of oceanic and atmospheric fugacities of CO_2, and parameterizations of the gas transfer velocity. In order to expand the global CO_2 flux data set, several automated underway systems have been installed on research vessels [e.g., *Wanninkhof and Thoning*, 1993; *Feely et al.*, 1998] or volunteer observing ships [e.g., *Cooper et al.*, 1998; *Murphy et al.*, 2001]. These systems make continuous measurements of the fugacity (or partial pressure) of CO_2 (fCO_2 or pCO_2) in subsurface waters and in the atmosphere. The difference in these fugacities (ΔfCO_2) is the driving force behind the flux of CO_2.

[3] Much of this effort is motivated by the necessity to quantify the global exchange of CO_2 between the atmosphere and ocean. The net global uptake of CO_2 was estimated by *Tans et al.* [1990] to lie between 0.3 and 0.8 Gt C yr^{-1}. These values were in contradiction to the tracer-calibrated oceanic models, which predicted global oceanic CO_2 uptake to be 2.2 ± 0.5 Gt C yr^{-1} [*Houghton et al.*, 1990]. *Sarmiento and Sundquist* [1992] suggested that some of the discrepancy could be accounted for by the presence of the cool skin at the ocean surface. The cool skin can alter the solubility of CO_2 in seawater through CO_2's temperature dependence.

[4] *Robertson and Watson* [1992] calculated the influence of the skin effect on the CO_2 flux. The skin temperature was

[1]Department of Applied Ocean Physics and Engineering, Woods Hole Oceanographic Institution, Woods Hole, Massachusetts, USA.
[2]Atlantic Oceanographic and Meteorological Laboratory, Miami, Florida, USA.
[3]Applied Physics Laboratory, University of Washington, Seattle, Washington, USA.
[4]Department of Chemistry, University of Montana, Missoula, Montana, USA.
[5]Cooperative Institute for Research in Environmental Sciences, University of Colorado, Boulder, Colorado, USA.

0148-0227/04/2003JC001800$09.00

derived from a parameterization from *Hasse* [1971]; the gas transfer velocity was calculated using the relationship from *Tans et al.* [1990]. After incorporating the skin effect into global CO_2 flux estimates, *Robertson and Watson* [1992] found ~0.7 Gt C yr^{-1} increase in global ocean CO_2 uptake.

[5] *Van Scoy et al.* [1995] extended this analysis to include a more realistic wind field, and determined that the skin-assisted CO_2 flux would be 40% lower than the value determined by *Robertson and Watson* [1992], when using a Rayleigh wind speed distribution. Furthermore, the use of a gas transfer velocity parameterization from *Liss and Merlivat* [1986] yielded a value of 0.17 Gt C yr^{-1} increase in the global CO_2 flux over that of *Tans et al.* [1990].

[6] *Wong et al.* [1995] presented seasonal estimates of the bias on the air-sea flux of CO_2 from the skin effect in the subtropical Pacific. He summarized this bias in four latitudinal bands from 45°N to 25°S. It was found that the relative increase in the flux ranged from +56% in the Austral Summer over 25°S–15°S to −71% in the Boreal Autumn over 25°N–35°N.

[7] The formation of a surface warm layer can also influence the air-sea flux of CO_2. The term "warm layer" was suggested by *Fairall et al.* [1996] to describe warming of the upper few meters of the ocean from solar radiation. *McNeil and Merlivat* [1996] examined how the diurnal variability of the warm layer can influence the CO_2 flux, having the effect of increasing evasion for oceanic source regions, and vice versa for sink regions.

[8] *Bates et al.* [1998] showed that temperature was the dominant control over seawater pCO_2 from diel to seasonal timescales in the Sargasso Sea, and that temperature could be used to extrapolate regional pCO_2 data to wider spatial scales using remotely sensed SST.

[9] According to these studies, temperature-related effects can substantially influence the global air-sea flux of CO_2. However, the magnitude of these effects have never been quantified with colocated in situ ΔfCO_2, cool skin, and warm layer observations. The GasEx-2001 experiment provided an opportunity to conduct such an analysis. In this paper we present results from the GasEx-2001 cruise with direct measurements of underway CO_2 fugacity, radiometric skin temperature, high-resolution profiles, and several point measurements from Lagrangian platforms. These data were used to investigate temperature-related biases on the air-sea CO_2 flux.

2. Air-Sea Exchange

[10] As the air-sea interface is approached from below, turbulence diminishes and molecular conduction becomes responsible for transfer processes. Large gradients of scalar quantities occur close to the surface in the absence of the mixing efficiency of turbulence [*Donelan and Wanninkhof*, 2002]. Figure 1 shows an idealized schematic of CO_2 concentration and temperature extending from a few meters below the surface out into the atmospheric boundary layer. The thermal sublayer (ΔZ_T) typically extends to about 1 mm in depth [*Mammen and von Bosse*, 1990]. The concentration sublayer (ΔZ_C) scales with the thermal sublayer as $(D_C/D_T)^{1/3}$, where D_C and D_T are the coefficients of diffusivity for gas and heat, respectively. These quantities have values

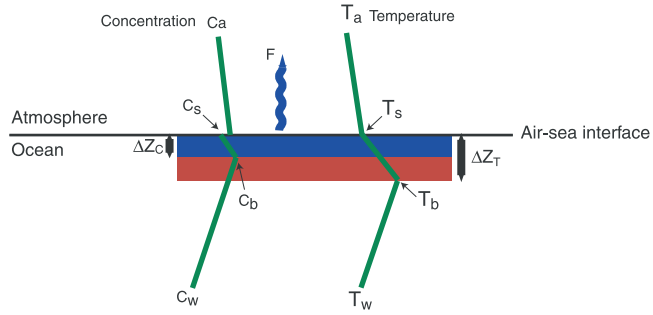

Figure 1. Schematic illustrating air-sea transfer and indicating the nomenclature for the measurements as a function of depth used in the text. The subscript "w" corresponds to measurements at the ship intake depth of approximately 5 m; "b" corresponds to the base of the molecular boundary layer; "s" corresponds to the skin measurements; "a" corresponds to measurements in the atmosphere.

of 2×10^{-9} and 1×10^{-7} m^2 s^{-1}, providing a ΔZ_C of about 250 μm, or about one fourth of the thermal sublayer [*Doney*, 1995].

2.1. Air-Sea Flux Of CO_2

[11] The air-sea exchange of gases obey Henry's law, which is the ratio between the aqueous-phase concentration of a species and its gas-phase concentration, i.e., $C_s \simeq C_a/K_H$. Here C_s is the concentration of CO_2 at the water surface, C_a is the atmospheric CO_2 concentration, and K_H is the dimensionless Henry's coefficient. The flux of CO_2 across the air-sea interface can be written as the difference in concentration in the aqueous phase across the diffusion sublayer [*Jacobs et al.*, 1999],

$$F = k_w[C_b - C_s], \tag{1}$$

where F is the CO_2 flux, C_b is the concentration at the base of the diffusion sublayer, and k_w is the transfer velocity (see Figure 1).

[12] The transfer velocity is parameterized in terms of wind speed [e.g., *Liss and Merlivat*, 1986; *Wanninkhof*, 1992; *Wanninkhof and McGillis*, 1999; *Nightingale et al.*, 2000]. The parameterization by *Wanninkhof* [1992] is given by

$$k_w = 0.31u_{10}^2(Sc/Sc_{20})^{-1/2}, \tag{2}$$

where u_{10} is the wind speed at 10 m and $Sc(T, S)$ is the dimensionless Schmidt number, a function of temperature and less importantly salinity; here it is referenced to a temperature of 20°C in seawater ($Sc_{20} \simeq 660$). The transfer velocity can also be determined by inverting equation (1) with direct measurements of F using the eddy correlation method [*McGillis et al.*, 2001].

[13] Calculation of the flux of CO_2 from the ship data require that equation (1) is rewritten as

$$F = k_w\alpha_w[fCO_{2w} - fCO_{2a}], \tag{3}$$

where α_w is the solubility of CO_2, and fCO_{2w} and fCO_{2a} are the fugacities of CO_2 in the water and atmosphere,

respectively. This expression is an approximation to equation (1) as it is technically unfeasible to determine the concentration of CO_2 across the diffusive boundary layer at the ocean-air interface.

2.2. Sea Surface Temperature Gradients

[14] The fact that $T_s < T_b$ in Figure 1 is a consequence of the way heat is exchanged between the ocean and atmosphere. The flux of latent heat acts only on the water surface providing cooling. During GasEx-2001, the sensible heat flux was out of the ocean, further cooling the surface. The longwave radiation is emitted over the upper few micrometers of the sea surface, reinforcing the cooling. The heat gain to the ocean is through shortwave radiation penetrating the upper ocean.

[15] The skin-bulk temperature difference is defined as $\Delta T = T_s - T_b$, but quite often the T_b measurement is unavailable due to lack of suitable instrumentation, and so is replaced with a more conveniently available temperature, usually at an arbitrary depth within the water column (denoted as T_w in Figure 1). *Ward and Minnett* [2002] have shown that failure to account for a vertically heterogeneous profile of bulk temperature can result in a large error in ΔT. The ΔT parameter has been the focus of several studies from a field observational perspective [e.g., *Jessup and Hesany*, 1996], from a satellite view of sea surface temperature (SST) [e.g., *Kearns et al.*, 2000], and under the context of modeling ΔT [e.g., *Wick et al.*, 1996].

2.3. Temperature Biases on CO_2 Flux

[16] There are several individual temperature biases that must be considered when correcting the air-sea CO_2 flux, as outlined below. It should be noted that the corrections described here come from four sources, and each are inter-related. However, each source is treated as stand alone for clarity. We combine the four biases into a single equation in section 2.3.5.

2.3.1. Solubility

[17] The solubility of CO_2 in seawater is determined from the data of *Weiss* [1974] and is a function of both temperature and salinity. The solubility of CO_2 in seawater drops by a factor of 2 over a 0–30°C range. The ubiquity of the cool skin at the sea surface dictates that the solubility-temperature dependence must be considered, requiring an additional term in equation (3),

$$\Phi_\alpha = k_w(\alpha_w - \alpha_s) f\mathrm{CO}_{2a}, \tag{4}$$

where Φ_α represents a modification in the CO_2 flux due to the influence of ΔT on the solubility, and α_s is the solubility of CO_2 calculated with the skin temperature. This results in a new equation for the CO_2 flux,

$$F_\alpha = k_w[\,\alpha_w fCO_{2w} - \alpha_s fCO_{2a}], \tag{5}$$

where F_α is the flux accounting for the cool skin effect. This is the only correction applied by *Robertson and Watson* [1992], *Van Scoy et al.* [1995], and *Wong et al.* [1995].

2.3.2. Water Vapor

[18] The underway $f\mathrm{CO}_2$ system outputs the mixing ratio of air XCO_{2a}, calculated for dry air. This value must be converted to fugacity, using the following relationship: $f\mathrm{CO}_{2s} = Xa\ (P - pH_2O)\ \exp[(B_{11} + 2\delta_{12})P/RT_s]$, where $f\mathrm{CO}_{2s}$ is the fugacity of CO_2 at the surface, P is the atmospheric pressure, pH_2O is the water vapor pressure, and the exponential term is the fugacity correction [*Wanninkhof and Thoning*, 1993]. The water vapor pressure and the virial coefficient are temperature dependent, and so pH_2O and B_{11} must be determined with T_s instead of T_w, as this is a surface measurement. This requires the following additive term to equation (3):

$$\Phi_X = k_w\alpha_w(f\mathrm{CO}_{2a} - f\mathrm{CO}_{2s}). \tag{6}$$

The corrected flux from equation (3) is now

$$F_X = k_w\alpha_w[fCO_{2w} - fCO_{2s}]. \tag{7}$$

2.3.3. Transfer Velocity

[19] The transfer velocity k_w incorporates both the diffusivity of the gas in water, which varies with temperature and between different gases, and also the effect of physical processes within the water boundary layer. The temperature dependence of k_w is through the Schmidt number in equation (2), defined as the ratio of the kinematic viscosity of water to the molecular diffusivity of CO_2 in water. Sc is approximated by a third-order polynomial fit to the water temperature [*Wanninkhof*, 1992]. The transfer velocity is the exchange parameter between the ocean and atmosphere, which is representative of the diffusive sublayer. The top of the molecular boundary layer is in direct contact with the atmosphere; thus the correct temperature with which it should be parameterized is T_s, i.e., $k_w = k_w[u_{10}, T_s] \equiv k_s$. This bias requires an additional term to equation (3), namely,

$$\Phi_k = \alpha_w[k_w(fCO_{2a} - fCO_{2w}) + k_s(fCO_{2w} - fCO_{2a})]. \tag{8}$$

This leads to the flux term

$$F_k = k_s\alpha_w[fCO_{2w} - fCO_{2a}]. \tag{9}$$

2.3.4. Seawater Fugacity

[20] Because of the CO_2 equilibria, seawater $f\mathrm{CO}_2$ exhibits a strong temperature dependency which has been determined by *Takahashi et al.* [1993]. By equilibrating a North Atlantic seawater sample over several temperatures, while the total CO_2 concentration, alkalinity, and salinity were kept constant, the fugacity was determined at each temperature. An exponential relationship between the fugacity and temperature was found. The least-squares fit to the natural logarithm of the $f\mathrm{CO}_2$ yielded $(\delta \ln f\mathrm{CO}_2/\delta T) = 0.0423 \pm 0.0002\ \mathrm{C}^{-1}$. Warm layer temperature gradients can thus affect the $f\mathrm{CO}_{2w}$ [*McNeil and Merlivat*, 1996], and this bias can be represented by a further additive term to equation (3),

$$\Phi_f = k_w\alpha_w e^{\gamma} f\mathrm{CO}_{2w}, \tag{10}$$

where $\gamma = 0.0423(T_b - T_w)$ and T_b and T_w are the temperatures at the base of the molecular boundary layer and the seawater fugacity measurement depth, respectively (see Figure 1). The term with α_b is the correction to the

solubility over the warm layer. The new CO_2 flux term after the warm layer modification is

$$F_f = k_w \alpha_w [fCO_{2w} e^{\gamma} - fCO_{2a}]. \quad (11)$$

2.3.5. Total Temperature Bias

[21] Equation (5) introduces the solubility calculated with T_s, as this is the water temperature immediately adjacent to the atmosphere. Equation (7) goes further by introducing the surface fugacity fCO_{2s}. However, the solubility term α_s does not appear in equation (7) as the intention is to determine each bias individually. Equation (9) introduces a further correction based on T_s, but neither of the previous corrected terms appear in equation (8). Finally, equation (11) investigates the warm layer as an individual bias to the CO_2 flux. It is necessary to combine these corrections into a single term. The result is

$$F_T = k_s [\alpha_b (f\mathrm{CO}_{2w} \mathrm{e}^{\gamma}) - \alpha_s f\mathrm{CO}_{2s}]. \quad (12)$$

The correct transfer velocity from equation (9) now appears in equation (12), as does the correctly determined surface fugacity fCO_{2s} from equation (7), which now has the surface solubility α_s associated with it. The correct determination for the aqueous fugacity is now present in equation (12).

3. GasEx-2001 Campaign

[22] One of the objectives of the GasEx-2001 experiment was to determine the magnitude and controls on the CO_2 gas transfer velocity in the equatorial Pacific. This region is one of the largest oceanic sources of CO_2, with an annual CO_2 flux of 0.5–1 Gt C yr^{-1} [*Takahashi et al.*, 1997]. The ΔpCO_2 in this region is on average +80 to +150 μatm.

3.1. Cruise Conditions

[23] GasEx-2001 was conducted on the NOAA ship *Ronald H. Brown* (RHB) in the eastern equatorial Pacific from February 15 to March 1, corresponding to yeardays (YD) 46–60. An array of drifters were deployed at the coordinates of 3°S 125°W, and recovered at 2.3°S 131.5°W, a distance of approximately 700 km.

[24] Figure 2a shows the temperature and salinity from the thermosalinograph on the RHB located at the ship intake ~5 m below the waterline. The seawater temperature reflects the diurnal modulation that was predominant in the GasEx-2001 region. It also shows that there is an average increase of ~0.7°C in temperature throughout the experiment. The salinity had an initial value of 35.1 ppt and remains almost invariant for the duration of the observational period, except for two large spikes on days 51 and 53. The latter was associated with a 24-hour regional survey. The former drop in salinity is associated with an intense rain event.

[25] The seawater and atmospheric fugacities are shown in Figure 2b. The effect of temperature on the fCO_{2w} is apparent. Throughout the experiment the average fCO_{2w} values decreased. The change in water mass when the ship moved away from the Lagrangian drifters is apparent in the fCO_{2w} record. The atmospheric fCO_2 measurements during the measurement period had a mean value of 354.4 ± 0.7 μatm. The oscillations in the fCO_{2a} were due to the atmospheric tide, which is strongest at the equator.

[26] The wind record is shown in Figure 2c. The wind speed was typical for this region, maintaining an average of about 6 m s^{-1}. The minimum wind speed was recorded on day 51 when it dropped to 3 m s^{-1}, and achieved a maximum of 11 m s^{-1} on day 53. The wind direction maintained an easterly direction throughout the observational period, with some occasional shifts to the southeast.

[27] Figure 2d shows the downwelling shortwave radiation as well as the sum of the heat loss components, i.e., sensible, latent, and longwave radiative fluxes. The insolation reached a daily maximum of over 1000 W m^{-2} except for days 48, 50, and 55, during this period. The sum of the outgoing heat fluxes increased slightly throughout the observational period, but never exceeded the daytime heating.

[28] All heat fluxes are defined as positive in the downward direction, and the skin-bulk temperature difference is negative for a cool skin. The CO_2 flux is defined as positive for oceanic supersaturation.

3.2. Fugacity Measurements

[29] The underway CO_2 system permanently installed on the RHB provides measurements of the fugacity of CO_2 dissolved in seawater, as well as that in the atmosphere [see *Wanninkhof and Thoning*, 1993]. The underway system measures the dried mixing ratio of CO_2; i.e., XCO_2, which is then converted to fugacity, using the equation referred to in section 2.3.2.

[30] Seawater is pumped from the ship intake to an equilibrator. Here the seawater is equilibrated with circulating air, which is then analyzed with an infrared analyzer to determine the XCO_{2w}. The atmospheric mixing ratio is measured by pumping a sample of ambient air from the bow of the ship (approximately 10 m above the surface) to the same infrared analyzer. A more detailed overview of the measurement system is given by *Wanninkhof and Thoning* [1993].

3.3. Temperature Measurements

[31] Seawater temperature was measured with several sensors during GasEx-2001. One of the measurement philosophies underlying GasEx-2001 was to minimize the influence of the research vessel, which was accomplished by deploying several Lagrangian platforms. These included an Air-Sea Interaction Spar (ASIS) buoy, to which was attached the Drogue drifter, and a Carbon Interface Ocean Atmosphere (CARIOCA) buoy.

[32] The Skin Depth Experimental Profiler (SkinDeEP), an upwardly rising autonomous profiler, provided bulk temperatures within the upper few meters of the ocean. A detailed description of SkinDeEP is given by *Ward et al.* [2004]. During GasEx-2001, SkinDeEP was equipped with an FP07 thermistor and a high-resolution conductivity sensor. A continuous time series was not available for SkinDeEP due to (1) the nature of the measurement, i.e., a continuous depth profile at discrete time intervals, and (2) limited supply of available power. The trade-off when deploying SkinDeEP is shorter profile intervals against longer deployment times. SkinDeEP was used for short-term (hours) high-resolution profiling of the upper few

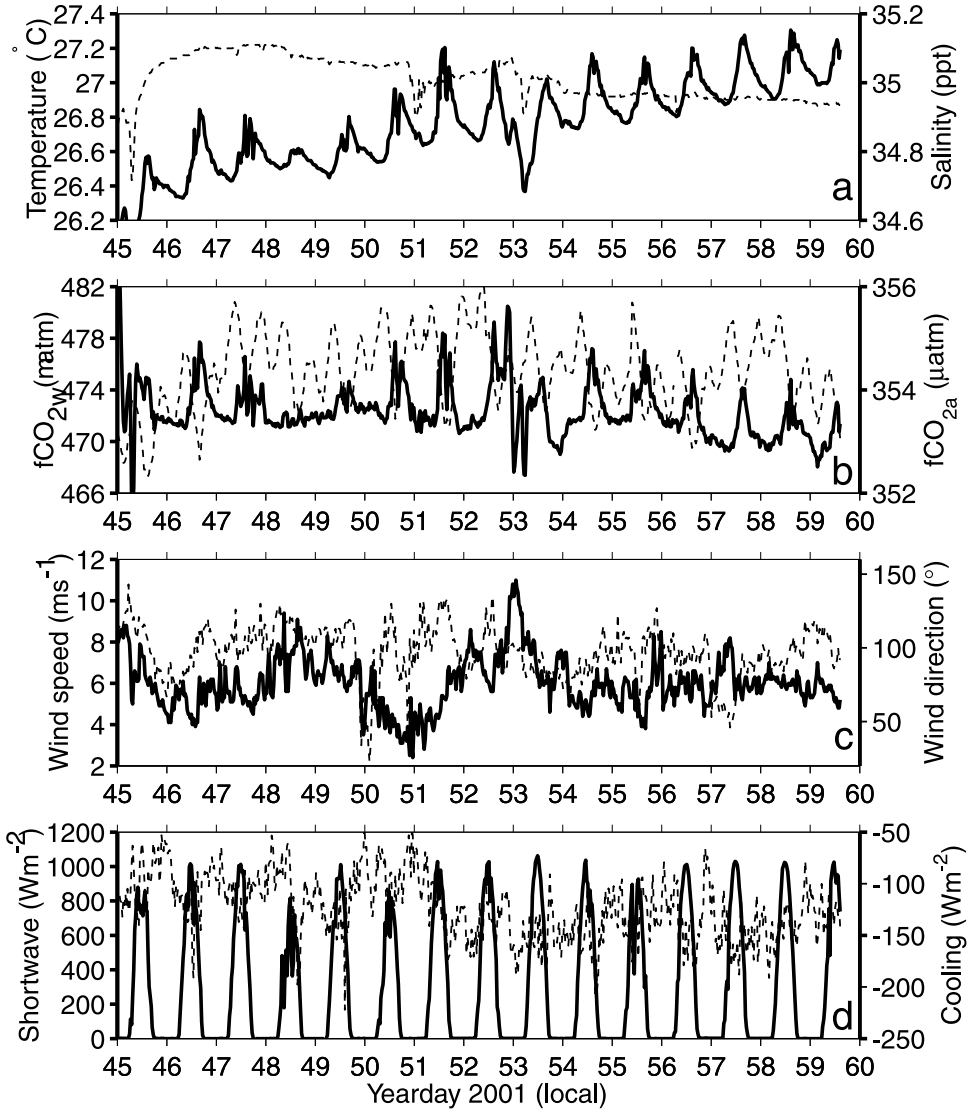

Figure 2. Thirty-minute-averaged data presenting conditions encountered during GasEx-2001: (a) Seawater temperature (solid line) and salinity (dashed line) from the RHB's thermosalinograph. (b) Aqueous (solid line) and atmospheric (dashed line) CO_2 fugacities from ship's underway system. (c) Wind speed (solid line) and direction (dashed line) from the RHB flux package. (d) Downwelling shortwave radiation (solid line) and surface cooling (dashed line), i.e., sum of sensible, latent, and net longwave fluxes.

meters. Several of the point temperature measurements were provided by other in situ temperatures also deployed on both ASIS and the Drogue.

[33] The skin temperature was measured by the Calibrated, InfraRed In situ Measurement System (CIRIMS), which provides calibrated temperature with an accuracy of 0.1°C [*Jessup et al.*, 2002]. In general, the accuracy in measuring T_s using CIRIMS is limited by the uncertainty in correcting the measured sea surface brightness temperature for reflected IR radiation from the sky. Sources of uncertainty in the sky correction include temporal variability due to partly cloudy conditions and surface roughness.

[34] The RHB thermosalinograph (TSG) recorded temperature and salinity continuously. The TSG temperature was compared to the CTD temperature, which was accurate to 0.5 mK (Greg Johnson, personal communication, 2002). For nighttime conditions, the mean temperature difference between the CTD and TSG was 0.02°C, with a standard deviation of 0.02°C. All in situ temperature measurements were accurate to within 0.05°C, compared to the TSG.

[35] A floating thermistor (Seasnake) was deployed throughout the campaign and consists of a thermistor embedded into a length of buoyant synthetic cord, allowing measurements within the upper few centimeters of the water. The accuracy of the Seasnake was 0.1°C.

[36] Table 1 indicates the platform on which the temperature measurements were made, the depth of the measurements, the logging interval, and the nomenclature used in the remainder of the text. There were four different platforms involved, two of which, ASIS and the Drogue, were physically attached to each other. The RHB remained within a few kilometers of the ASIS/drogue array, except during

Table 1. Temperature Sensors Deployed in the Upper 5 m of the Water Column During GasEx-2001

Platform	Sensor	Logging Interval, s	Nominal Depth, m	Nomenclature
SkinDeEP	FP07	~200	~7–0	T_{SD}
R/V RHB	CIRIMS	1800	0	T_{skin}
R/V RHB	Seasnake	600	0.1	T_{SS}
R/V RHB	TSG	60	5	T_{TSG}
ASIS	SAMI 4	1800	1	T_{A1a}
ASIS	SAMI 11	1800	1	T_{A1b}
ASIS	YSI 904	1800	1	T_{A1c}
ASIS	SAMI 15	1800	5	T_{A5}
Drogue	YSI 400	1800	1	T_{D1}
Drogue	YSI 583	1800	4	T_{D4a}
Drogue	SAMI 16	1800	4	T_{D4b}

the "butterfly" pattern survey. SkinDeEP did not record location, but generally followed in the same direction as the drifting array.

4. Results

4.1. Individual Biases

[37] Figure 3a shows a histogram of the SkinDeEP deployments. Although measurements from SkinDeEP were not evenly distributed throughout the 24-hour period, deployments of SkinDeEP covered the nearly full range of wind speeds. The deployment times were skewed toward the afternoon and evening, with the smallest amount of data being available between the hours of midnight and midday.

[38] In order to investigate the individual temperature biases described in section 2.3, the data from the SkinDeEP profiler, the CIRIMS radiometer, and the underway pCO_2 system are utilized. Under this scheme, the pCO_2 and CIRIMS data are interpolated to the SkinDeEP measurement times. The remaining subplots in Figure 3 present the quantity Φ/F, where Φ is calculated from either equations (4), (6), (8), or (10), and F is calculated according to equation (3). This is the relative change in the flux from the temperature-induced biases. These quantities are plotted against wind speed as this is one of the primary sources of turbulence at the air-sea interface. The flux of CO_2 increases with wind through equation (2). Temperature gradients diminish with wind leading to a homogeneous bulk temperature and smaller ΔT. The colored data points in Figures 3b–3e correspond to the time of day shown in the histogram in Figure 3a.

[39] Figure 3b shows the solubility bias from equation (4) plotted against wind. There is a cool skin present during the periods when these data were acquired, which results in a retardation of the CO_2 flux. The magnitude of this bias decreases with increasing wind speed. This bias reaches a maximum of about 4% during the daytime hours at low wind speeds.

[40] Figure 3c shows the wind speed dependence of the transfer velocity bias Φ_k in equation (8) expressed as a percentage of the unadjusted CO_2 flux in equation (3). The skin temperature correction on the transfer velocity shows a similar pattern to Figure 3b, but with a smaller magnitude. Temperature biases resulting from modification of k range from a maximum of −1.5% at low winds, to zero toward higher winds.

[41] The smallest temperature bias results from the water vapor bias, i.e., recalculation of the fugacity with T_s instead of T_w according to equation (6). This is presented in Figure 3d. There is a weak wind speed dependence with a maximum enhancement of only 0.3%.

[42] The bias introduced to the flux of CO_2 from the formation of the warm layer in equation (10) is shown in Figure 3e. The temperature T_w at 5 m depth is where the fCO_{2w} was measured with the underway system. The temperature difference across the warm layer is determined from the surface temperature measurement on SkinDeEP. This difference in temperature was used to determine the quantity Φ_f in equation (10). During GasEx-2001, the water was supersaturated in CO_2, and therefore increases in temperature toward the surface enhance the CO_2 evasion. The maximum enhancement of the flux occurs during the daytime and early evening (denoted by the red and blue data points) in combination with low wind speeds, which correspond to the conditions where maximal stratification occurs. During the hours when there is no shortwave radiation present, there is a zero flux enhancement, corresponding to a well-mixed water column. Figure 3e also shows a decreasing bias on the flux as the wind speed increases.

[43] Figure 3f shows the combined effects of temperature on the flux of CO_2, i.e., equation (12). The overall temperature bias is dominated by the presence of the warm layer, which is at a maximum of about +4% during low winds and periods of high insolation. The nighttime bias, primarily from the cool skin effect, is less dependent on wind speed and reduces the flux to by a mean value of about −2%.

4.2. Cool Skin Effect

[44] This section investigates the cool skin and the effect on the CO_2 flux, utilizing the full time series during the observational period. A time series plot of the skin effect $\Delta T = T_s - T_b$ is shown in Figure 4a. There are two approximations for bulk temperatures in this plot: the thermosalinograph (T_w) and the Seasnake (roughly equivalent to T_b). The skin temperature (T_s) data are from the CIRIMS radiometer. The time axis is local solar time, where noon is chosen as the time when the sun is at its maximum height for the local co-ordinates. Throughout this time series, the TSG-derived ΔT is smaller than the Seasnake-derived ΔT. This would indicate the cooling at the surface is stronger than the warming from insolation. The occurrences of a warm skin temperature are practically zero for the ΔT referenced to the TSG.

[45] Figure 4b shows the skin temperature influence on the CO_2 flux from the combined effects described in equations (4), (8), and (6). There is a net lowering of CO_2 evasion due to the predominantly cool skin, with a maximum of almost 4%.

4.3. Parameterizations of ΔT

[46] Our measured skin temperature can be compared to a variety of theoretical models. There exist many parameterizations to predict the bulk-skin difference at the sea surface. *Wick et al.* [1996] provides a summary of the available parameterizations. All previous studies of the effect of ΔT on the gas flux [*Robertson and Watson*, 1992; *Wong et al.*, 1995; *Van Scoy et al.*, 1995] have

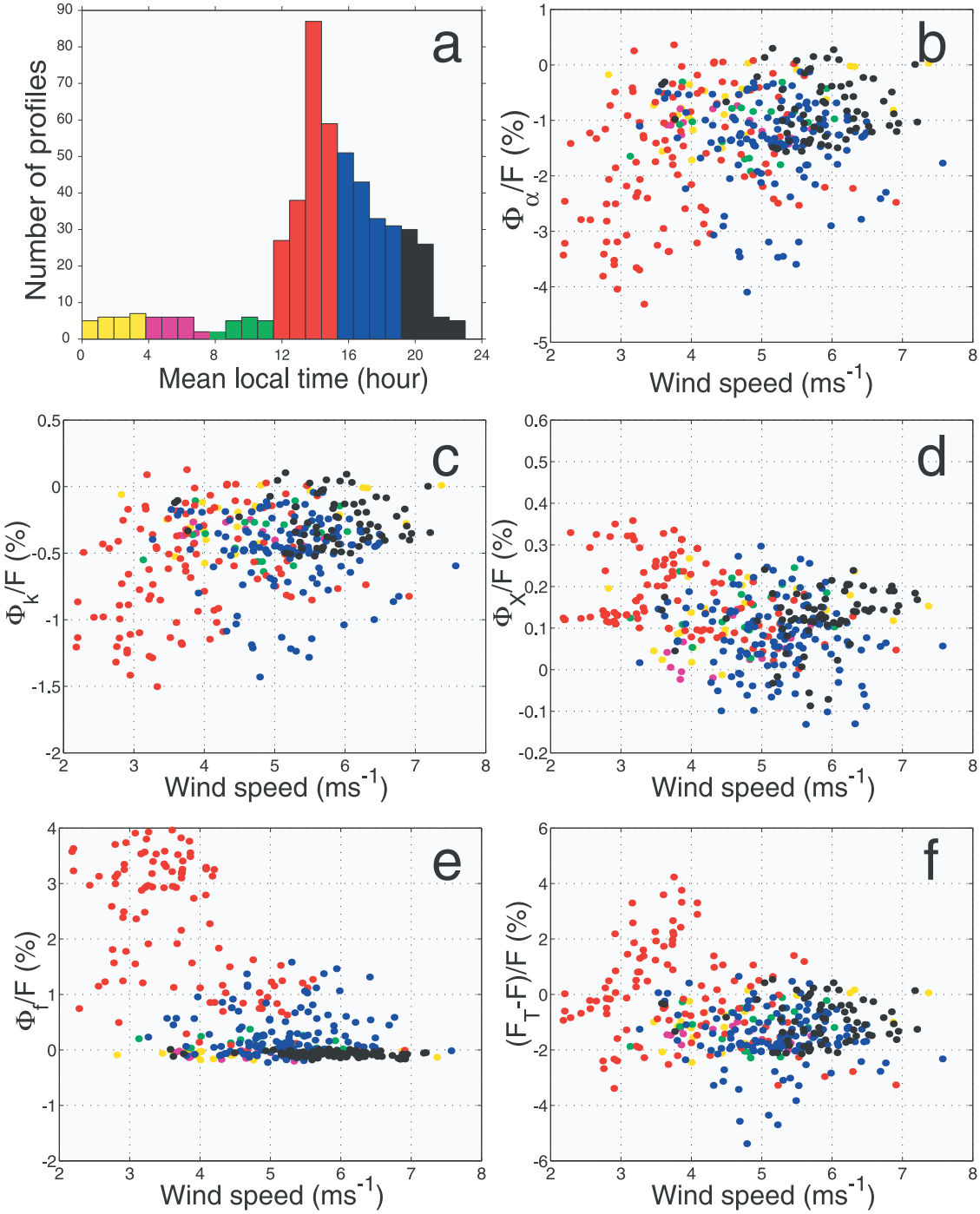

Figure 3. (a) Histogram for the local times of day that SkinDeEP was deployed. The colored data points in Figures 3b–3f correspond to these times of day. Wind speed dependence of the relative increase in the CO_2 flux resulting from (b) skin temperature solubility calculation in equation (4), (c) Schmidt number calculation based on T_s in equation (8), (d) calculation of fugacity in air from the mixing ratio in equation (6), (e) calculation of the increase in fCO_2 from the warm layer in equation (10), and (f) combined temperature-related biases on the air-sea flux of CO_2 from equation (12).

employed the parameterization by *Hasse* [1971], which assumes a linear temperature drop across the thermal boundary layer. We investigate the Hasse parameterization (HAS) here, as well as two other physically disparate parameterizations: *Schlüssel et al.* [1990] (SCH), an empirical model based on data from the North Atlantic, and *Soloviev and Schlüssel* [1996] (SOLSCH), which employs surface renewal theory.

4.3.1. Hasse

[47] The parameterization by *Hasse* [1971] used a diffusion model based on the flow patterns seen at rigid wall boundaries where the efficiency of turbulent diffusion

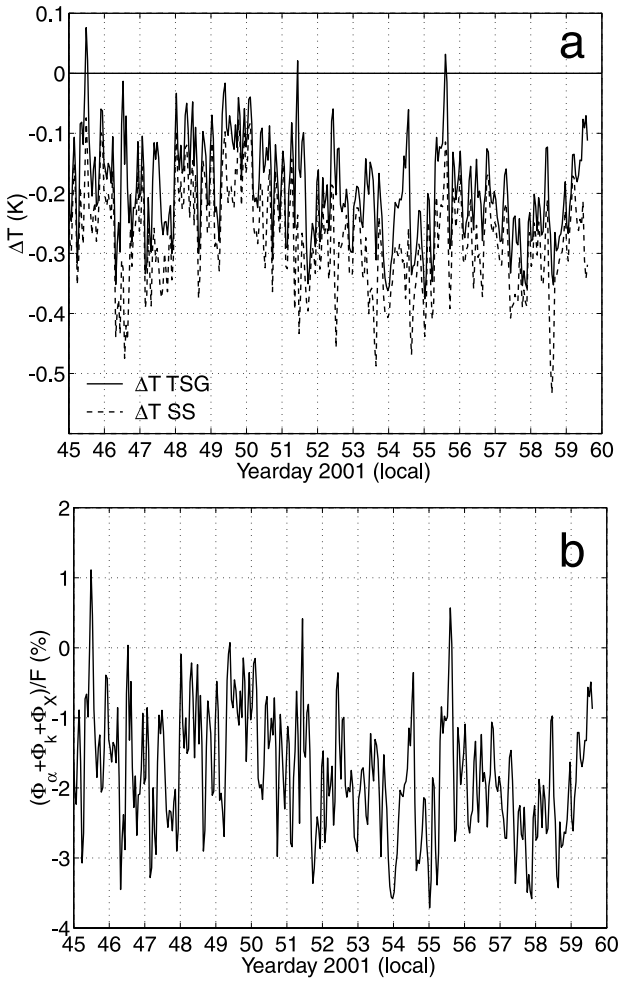

Figure 4. (a) Skin-bulk temperature differences for the thermosalinograph (T_{TSG}) and Seasnake (T_{SS}) bulk temperatures. (b) Bias introduced into the CO_2 flux after skin temperature correction from equations (4), (8), and (6).

decreases as the wall is approached. Hasse assumed that there were two layers: one where the water thermal diffusivity could be approximated by molecular diffusivity, and a second layer where the eddy diffusivity was appropriate. The temperature deviation for the two layers from 134 temperature profiles was plotted and it was found that for practical use, the temperature deviation was well represented by

$$\Delta T = c_1 \frac{q_0}{u_{10}} + c_2 \frac{q_R}{u_{10}}, \tag{13}$$

where $q_0 = q_L + q_S + q_T$ and is the sum of the latent, sensible, and net longwave radiative heat fluxes, u_{10} is the wind speed corrected to 10 m, and q_R is the net shortwave radiation. The coefficients c_1 and c_2 are dependent on the depth at which the bulk temperature is measured. The first term on the right-hand side of equation (13) is the nighttime ΔT, and the second term includes the shortwave component q_R to the heat flux.

[48] A scatterplot of the measured ΔT_{TSG} against the Hasse-parameterized ΔT is shown in Figure 5a. The parameterization overestimated the ΔT during daylight hours, and underestimated it during the nighttime. The mean difference between the measured ΔT is -0.031C, with a standard deviation of 0.16C, and a correlation coefficient of 0.44.

[49] The corresponding relative increase in the CO_2 flux for the parameterized ΔT is shown in Figure 5b. There is a strong diurnal signal to the CO_2 flux bias, with flux enhancements during the afternoon where the effects of insolation is at its peak. During the nighttime, the Hasse parameterization reduces the CO_2 flux by almost 4%.

4.3.2. Schlüssel et al.

[50] *Schlüssel et al.* [1990] developed an empirical model for ΔT where the fluxes and wind speed were entered into a multiple regression function. The coefficients were derived from North Atlantic observations of radiometric skin temperature, bulk water temperature, radiative fluxes, and meteorological variables. The expression for ΔT was found to be

$$\Delta T = a_0 + a_1 q_R/u_{10} + a_2(q_s - q_a) + a_3 q_T, \tag{14}$$

where q_s and q_a are water vapor mixing ratios of the sea surface and in the atmosphere. The coefficients are [*Soloviev and Schlüssel*, 1996] $a_0 = -0.467$ K, $a_1 = -0.00329$ km^3 s^{-1}W^{-1}, $a_2 = 97.428$ K, $a_3 = -0.00215$ km^{-2} W^{-1}.

[51] Figure 5c shows *Schlüssel et al.*'s [1990] parameterization for predicting the ΔT. The mean difference is -0.33C, with a standard deviation of 0.16C and a correlation coefficient of 0.46. Although the distribution is very similar to HAS, There is a large offset between the parameterized and measured ΔT.

[52] *Schlüssel*'s [1990] parameterized skin temperature introduces a much stronger positive bias to the CO_2 flux than that which was measured (Figure 5d). There is also a strong diurnal modulation to the bias. In this case, the CO_2 flux bias reaches a maximum of almost 8% during peak solar heating.

4.3.3. Soloviev and Schlüssel

[53] This parameterization is an extension of a previously developed model [*Soloviev and Schlüssel*, 1996], but includes the heating due to insolation. The parameterization assumes that the temperature drop across the molecular sublayer is from the combination of absorption of shortwave radiation and surface cooling. The solar absorption is modeled by a sum of exponentials after *Paulson and Simpson* [1981]. The surface cooling is based on surface renewal theory, where the molecular sublayers at the ocean surface are periodically destroyed, thereby eliminating the gradients that have been established there.

[54] ΔT is defined as $\Delta T(z, t) = \Delta T_c(z, t) + \Delta T_r(z, t)$ where ΔT_c and ΔT_r are the bulk-skin temperature differences due to surface cooling and absorption of solar radiation, respectively, and are a function of depth z, and surface renewal time t. These values are given as

$$\Delta T_c = \frac{4}{3} q_N \left(\frac{t}{\kappa\pi}\right)^{1/2}, \tag{15}$$

where κ is the coefficient of thermal molecular diffusion, and $q_N = q_0/(c_p\rho)$ is the normalized heat flux, and c_p and ρ are the specific heat capacity and density, respectively.

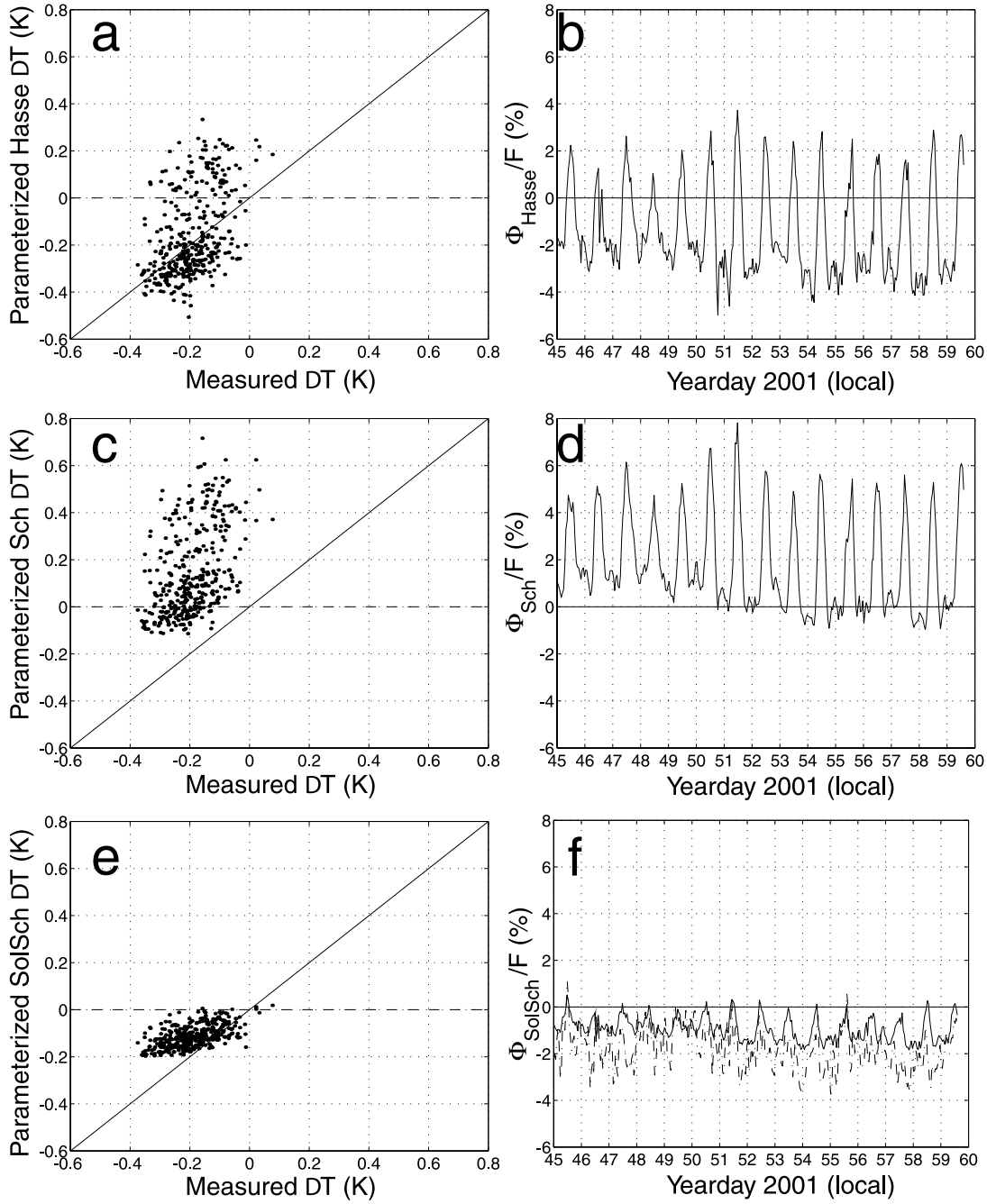

Figure 5. (left) Scatterplots of parameterized ΔT against that of the measured ΔT from (a) *Hasse* [1971], (c) *Schlüssel et al.* [1990], and (e) *Soloviev and Schlüssel* [1996]. The solid line approaches the ideal model. (right) Time series of the relative increase in the CO_2 flux from equation (3) for (b) *Hasse* [1971], (d) *Schlüssel et al.* [1990], and (f) *Soloviev and Schlüssel* [1996]. Figure 5f also contains the data from Figure 3b for comparison between the measured (dashed line) and parameterized (solid line) data. The data here are hourly averages.

[55] The quantity ΔT_r is given by

$$\Delta T_r = \frac{q_R(0)}{\kappa}\sum_{i=1}^{n} F_i\zeta_i^{-1} \cdot \left\{\exp\left(\delta_i^2\right)[1-\mathrm{erf}(\delta_i)] - 1 + 2\delta_i\pi^{-1/2} - \delta_i^2\right\}\delta_i^{-2} + \frac{4}{3}q_R(0)\frac{t}{\kappa\pi}^{1/2}, \quad (16)$$

where n = 9 is the number of wavelength bands from 200 nm to 3 μm, F_i is the fraction of shortwave radiation in each band, and ζ_i is the corresponding attenuation lengths (see *Paulson and Simpson* [1981] for these data). The quantity $\delta_i = \zeta_i(\kappa t)^{1/2}$ is the non-dimensional time. The net shortwave radiation at the ocean surface is denoted by $q_R(0)$.

[56] The parameterized ΔT is plotted in Figure 5e against the measured ΔT. The mean difference, standard deviation, and correlation coefficient are −0.08°C, 0.07°C, and 0.57,

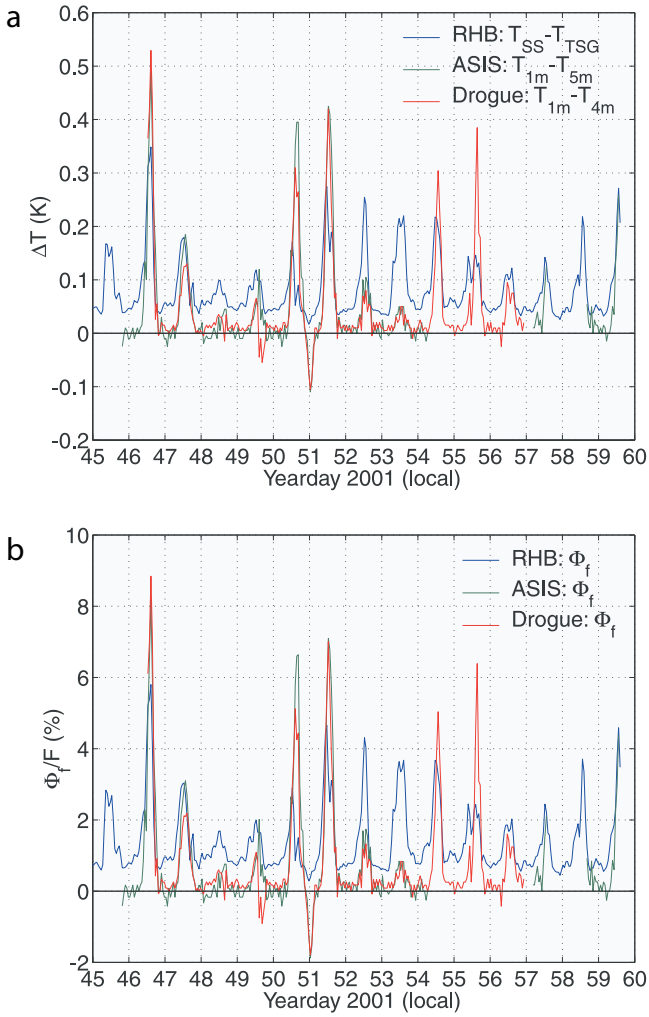

Figure 6. (a) Temperature differences across the warm layer for three platforms during GasEx-2001 (see Table 1). (b) Corresponding relative increase in the flux of CO_2 according to equation (10).

respectively. The parameterization tends to overestimate the measured ΔT, especially for $\Delta T < -0.2$. The bias on the CO_2 flux from the SOLSCH parameterization is slightly smaller than the measured bias, predicting a maximum retardation of the flux by only −1.8%.

4.4. Warm Layer Effect

[57] Figure 6a is a time series of three sets of temperature differences from the RHB, ASIS, and Drogue platforms (Table 1). Each of the series is the temperature difference between two sensors displaced by a few meters, but both located within the bulk. Thus these data provide a measurement of the temperature difference across the warm layer. The RHB data are taken from the TSG and the Seasnake, the ASIS data from two SAMI-pCO_2 sensors, and the Drogue data from two YSI sondes. There is a complete time series available from RHB, but there are gaps in ASIS data due to recovery of the instruments for maintenance and data offload. The last 3 days of Drogue data are missing due to exhaustion of battery power.

[58] The RHB data do not collapse to zero at nighttime, and thus indicates that there may be either a calibration issue, or that the proximity of the Seasnake to the RHB may be introducing some artificial warming. The ASIS and Drogue data are in fairly good agreement. However, there are disparities in the magnitude of the warming between the RHB data and that of ASIS/Drogue. On days 46, 50, 51, 54, and 55 the ASIS/Drogue data show stronger warming than the RHB data, and the converse is true for days 52 and 53. This would indicate horizontal inhomogeneities in the temperature field. The lack of agreement may also indicate shadowing effects, either on the RHB or the ASIS/Drogue. An inversion in the temperature difference occurred around local midnight on day 51, and it is more pronounced in the ASIS/Drogue data than the RHB. This cooler surface layer is coincident with a sharp drop in salinity of about 0.2 ppt from the rain event, which may have caused the colder water at 5 m to displace the warmer water at the surface. This inversion also coincided with the lowest wind speed encountered during the observational period.

[59] Figure 6b shows the effect of the warm layer on the CO_2 flux according to equation (10) for the three platforms. The data show a consistent enhancement of the flux, with maximums occurring around local noon.

[60] The ASIS/Drogue data show higher amplitudes in the enhancement when compared to the RHB, exceeding 6% on 4 out of the 15 days. The maximum addition to the flux from the ASIS/Drogue measurements exceeded 8% on day 46. The mean enhancement to the flux from ASIS was 0.73%, which was marginally lower than the Drogue mean value of 0.77%. The RHB had a mean enhancement value of 1.37%, with an offset of about 0.3%. These mean values include both day and nighttime periods. At the beginning of day 51, there is a negative influence on the CO_2 flux from the Lagrangian platforms, reducing the flux by 2%.

4.5. Warm Layer Model

[61] *Fairall et al.* [1996] developed a model to account for the warm layer, with a skin-bulk parameterization included. The warm-layer model was based on the 1-d model from *Price et al.* [1986]. Evolution of diurnal heating throughout the day leads to a critical point when the insolation exceeds the evaporative, sensible, and longwave cooling at the interface. Once this occurs, surface inputs of heat and momentum are confined to critical depth, predicted by the model. The warm layer model (WLM) provides the temperature difference across the warm layer.

[62] Figure 7 shows the results of the WLM, along with the RHB and ASIS temperature measurements. The model overestimates the warm layer on each day except for days 46 and 48. The largest discrepancies between the modeled and observed data are on days when the wind speed is low, indicating that the WLM is quite sensitive to wind-induced forcing. At nighttime, the WLM temperature collapses back on the TSG temperature.

5. Discussion

[63] During GasEx-2001, there was a consistent cool skin with respect to the bulk temperatures at different depths (Figure 4). There were three very brief periods when the skin temperature was greater than the temperature from the

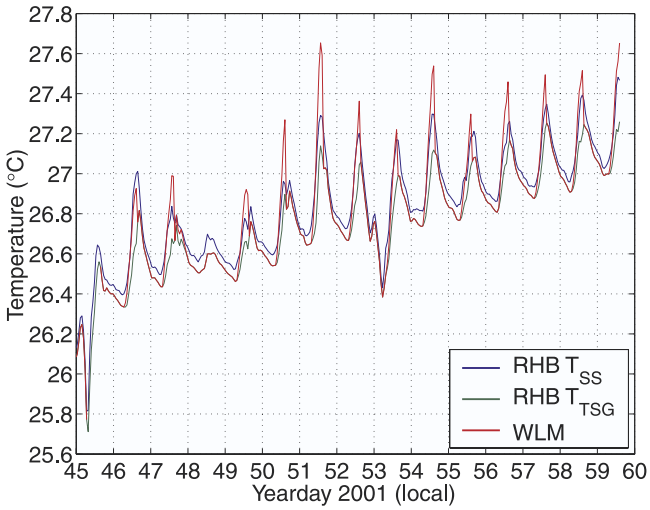

Figure 7. Time series of Seasnake (T_{SS}), thermosalinograph (T_{TSG}), and modeled (WLM) temperatures during GasEx-2001.

thermosalinograph, and this occurred shortly after peak insolation. The bulk temperature close to the surface (i.e., the Seasnake) never exceeded the skin temperature throughout the observational period. This would indicate that the cooling at the surface from the combination of sensible, latent, and longwave radiative fluxes was stronger than the warming from net shortwave radiation.

[64] Three ΔT parameterizations which incorporated the presence of shortwave radiation were employed in this study to determine which might be the most appropriate under conditions where radiometric skin measurements were not available. The parameterized ΔT was compared to the measured ΔT, but with the TSG temperature as the bulk value. This scheme is usually only appropriate at nighttime, where there is a homogeneous temperature profile with depth. However, the parameterizations were relatively successful in predicting ΔT during GasEx-2001 due to the strong cooling at the surface (Figure 5).

[65] Of the three parameterizations employed, the most successful was that of *Soloviev and Schlüssel* [1996]. However, this parameterization did not capture the maximum cooling of the skin temperature, and therefore the corresponding flux adjustment is influenced. The *Hasse* [1971] parameterization produced relatively small errors during the nighttime, but its ability to predict the measured ΔT during periods of insolation was poor (Figure 5a). However, Hasse's expression in equation (13) is far more accessible for incorporation into data analysis than Soloviev and Schlüssel's, and so it is understandable that this has been chosen in previous studies [*Schlüssel et al.*, 1990]. This empirical model did most poorly from the data acquired in the equatorial Pacific, which is not altogether surprising as these coefficients were determined from data measured in the northeast Atlantic Ocean.

[66] The WLM after *Fairall et al.* [1996] tended to overestimate the magnitude of the warm layer. This model relies on accurate determination of the shortwave absorption within the viscous boundary layer. This is achieved by using the *Paulson and Simpson* [1981] model. However, a recent study by G. A. Wick et al. (Improved oceanic cool skin corrections using a refined solar penetration model, submitted to *Journal of Physical Oceanography*, 2004) has shown that the solar transmission model after *Ohlmann and Siegel* [2000] provides an improved prediction of the warm layer temperature profile and corresponding heat flux components. The parameterization incorporates effects from solar geometry, cloud cover, and chlorophyll concentration. During GasEx-2001, it was found that adjustment of the coefficients of the Jerlov bulk absorption model, derived from chlorophyll profiles, allowed more accurate determination of the mixed layer temperature (Peter Strutton, private communication, 2002). The adjustment resulted in a distribution of short wave over a greater depth.

[67] The data from the SkinDeEP profiler allowed investigation into the individual temperature biases introduced into the CO_2 flux (Figure 3). The magnitude of the individual temperature biases show that during GasEx-2001 the warm layer influence, along with the solubility recalculation from the skin temperature, had the largest effect. The temperature influence on the transfer velocity was marginal, with the fugacity calculation effect being negligible. However, the data acquired by SkinDeEP was limited, and were not evenly distributed in time.

[68] Figure 8 shows a series of profiles over the upper 5 m from all of the data described in Table 1. This sequence was chosen because of the availability of SkinDeEP profiles during this period. Also shown are the results from the WLM/CSP model. The profiles extend from early afternoon into the nighttime from top to bottom. Each subplot presents the SkinDeEP data available for one hour, along with hourly averages of the remaining temperature measurements. The individual RHB data points (T_{TSG}, T_{SS}, and T_{skin}), ASIS/Drogue data points (T_{A1a}, T_{A1b}, T_{A1c}, T_{A5}, T_{D1}, T_{D4a}, T_{D4b}), and WLM/CSP data points allow for crude profiles to be generated through linear interpolation. The WLM assumes a linear profile of temperature of with depth. The evidence of the warm layer is seen in the RHB data up to 1739 LST. The WLM/CSP predicts that the warm layer will diminish after 1439 LST. The ASIS data show evidence of stratification until 1839 LST, but only in the 4-5 m depths.

[69] During the warm-layer periods, the SkinDeEP data exhibit a large variance between the profiles, but as the insolation diminishes throughout the day, the SkinDeEP data collapse back to a well-mixed situation with little variance. The three subplots up to 1539 LST show a temperature profile that is not linear with depth. The profile method eliminates calibration issues between several sensors, which is especially pertinent with requirements of at least 0.1C for studies of small-scale temperature variability close to the ocean surface.

6. Conclusions

[70] The analysis conducted here investigates the influence of the oceanic cool skin and the warm layer on the air-sea flux of CO_2 with direct observations from the Equatorial Pacific GasEx-2001 campaign. The data set involved measurements from the underway CO_2 system installed on the RHB, the SkinDeEP autonomous profiler, the CIRIMS radiometer, and several other point temperature measurements deployed on the Lagrangian platforms.

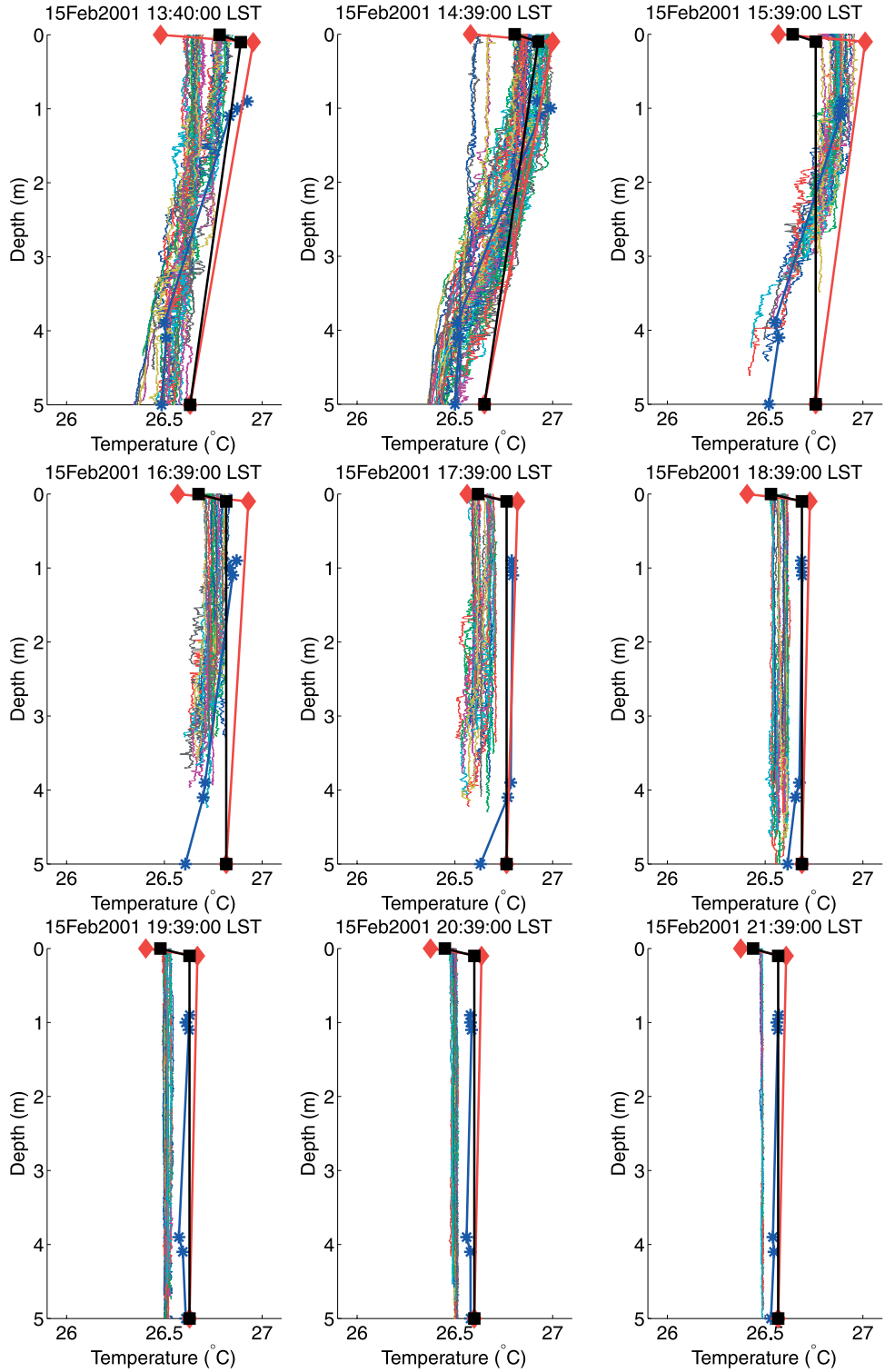

Figure 8. A series of temperature profiles from measurements on the RHB (diamond) using temperature data from the thermosalinograph, Seasnake, and CIRIMS skin temperature; ASIS/Drogue (asterisk) using data from the SAMI-pCO_2 sensors and YSI sondes; WLM/CS (square) modeled data. The high-resolution profiles are the SkinDeEP measurements. It should be noted that there were fewer profiles available during the latter part of the day.

[71] The relative increase in the CO_2 flux (i.e., $\Delta F/F$) from temperature in this study is quite small (Figure 3). This is a consequence of the large air-sea CO_2 fugacity difference in the equatorial Pacific. In other regions where the ΔfCO_2 (and hence the flux) is smaller, the relative increase in the CO_2 flux is greater from temperature biases is greater. The data in Figure 9 show an aqueous fCO_2 of 520 μatm and a warm layer ΔT of approximately 1°C. The relative increase

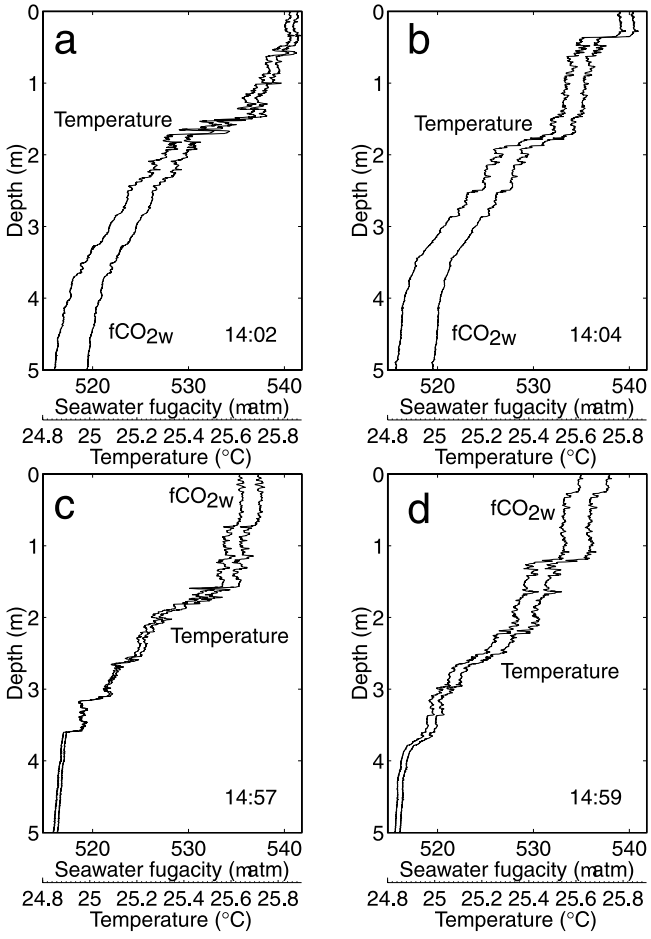

Figure 9. A series of SkinDeEP temperature profiles acquired on February 8 (YD 39) and the extrapolation of the aqueous fCO_2 to the surface from equation (10). The local times are indicated for each plot.

in the flux due to temperature is only about 4%, but this corresponds to an absolute increase of >20 μatm. However, when considered on a global scale, where the ΔfCO_2 is about 7 μatm [*Feely et al.*, 2001], this represents a substantial increase in surface water fCO_2.

[72] During GasEx-2001, the net effect from the cool skin and warm layer biases tended to cancel each other. However, this conclusion should not be extrapolated to a global situation. The eastern equatorial Pacific is a region where there is a significant amount of insolation, leading to thermal stratification in the near-surface layers of the ocean. The warm layer will bias the air-sea flux of CO_2 whenever present. Stratification occurs in regions where there is large insolation and small mixing. This tends to occur in the lower latitudes, and during the summertime in the higher latitudes. The one region where the warm layer will have the least significance on the CO_2 fluxes is the Southern Oceans, where the winds speeds tend to be relatively high, suppressing conditions of stratification. The absolute affect on the air-sea flux will be small however because the warm layer bias is only important at low wind speeds when rates of exchange are low.

[73] The cool skin, on the other hand, is persistent on a global basis [*Donlon et al.*, 2002], and will thus influence the air-sea flux of CO_2 in a more consistent fashion than the warm layer. During GasEx-2001 the relative increase retarded the flux out of the ocean by 4%. This cannot be considered to be globally representative because of the unique conditions in the equatorial Pacific of very high ΔfCO_2. In order to better understand the global influence of the skin temperature on the CO_2 fluxes, further in situ studies are necessary. This would require coincident observations of underway CO_2 fugacities with well-calibrated radiometers, i.e., with accuracies of better than 0.1C. Recently some efforts have been made in this direction through the installation of a CIRIMS on the RHB, along with two through-the-hull temperature/pressure sensors at 2 and 3 m below the waterline (A. T. Jessup, personal communication, 2003).

[74] The presence of near surface concentration gradients complicate the direct measurement of air-sea CO_2 fluxes. *Jacobs et al.* [2002] examined the disparity between the deliberate dual tracer (DDT) and the eddy covariance (EC) techniques for determination of the air-sea transfer velocity. Using model simulations, results showed that the DDT underestimated k_s by 10–25%, and that inconsistencies in the EC results could be introduced from varying fine-structure within the upper few meters of the ocean. These results provides an incentive to make near-surface ocean measurements if we are to improve estimates of CO_2 flux and rate of gas transfer.

[75] **Acknowledgments.** The authors acknowledge the officers and crew of the NOAA ship Ronald H. Brown for all their assistance during the GasEx-2001 campaign. This material is based upon work supported by the NSF under grant OCE-9986724, and by NOAA/OGP grant GC00-226. This paper is Woods Hole contribution 10855.

References

Bates, N. R., T. Takahashi, D. W. Chipman, and A. H. Knap (1998), Variability of pCO_2 on diel to seasonal timescales in the Sargasso Sea near Bermuda, *J. Geophys. Res.*, *103*, 15,567–15,585.

Cooper, D. J., A. J. Watson, and R. D. Ling (1998), Variation of pCO_2 along a North Atlantic shipping route (U.K. to the Caribbean): A year of automated observations, *Mar. Chem.*, *60*, 147–164.

Donelan, M. A., and R. Wanninkhof (2002), Gas transfer at water surfaces: Concepts and issues, in *Gas Transfer at Water Surfaces*, *Geophys. Monogr. Ser.*, vol. 127, edited by M. Donelan et al., pp. 1–10, AGU, Washington D. C.

Doney, S. (1995), Irreversible thermodynamics and air-sea exchange, *J. Geophys. Res.*, *100*, 8541–8553.

Donlon, C. J., P. J. Minnett, C. Gentemann, T. J. Nightingale, I. J. Barton, B. Ward, and M. J. Murray (2002), Toward improved validation of satellite sea surface skin temperature measurements for climate research, *J. Clim.*, *15*, 353–369.

Fairall, C. W., E. F. Bradley, J. S. Godfrey, G. A. Wick, J. B. Edson, and G. S. Young (1996), Cool-skin and warm-layer affects on sea surface temperature, *J. Geophys. Res.*, *101*, 1295–1308.

Feely, R. A., R. Wanninkhof, H. B. Milburn, C. E. Cosca, M. Stapp, and P. P. Murphy (1998), A new automated underway system for making high precision pCO_2 measurements onboard research ships, *Anal. Chim. Acta*, *377*, 185–191.

Feely, R. A., C. L. Sabine, T. Takahashi, and R. Wanninkhof (2001), Uptake and storage of carbon dioxide in the ocean: The global CO_2 survey, *Oceanography*, *14*, 18–32.

Hasse, L. (1971), The sea surface temperature deviation and the heat flow at the air-sea interface, *Boundary Layer Meteorol.*, *1*, 368–379.

Houghton, J. T., G. J. Jenkins, and J. J. Ephraums (1990), *Climate Change: The IPCC Scientific Assessment*, Cambridge Univ. Press, New York.

Jacobs, C. M. J., W. Kohsiek, and W. A. Oost (1999), Air-sea fluxes and transfer velocity of CO_2 over the North Sea: Results from ASGAMAGE, *Tellus, Ser. B*, *51*, 629–641.

Jacobs, C., J. F. Kjeld, P. Nightingale, R. Upstill-Goddard, S. Larsen, and W. Oost (2002), Possible errors in CO_2 air-sea transfer velocity from deliberate tracer releases and eddy covariance measurements due to

near-surface concentration gradients, *J. Geophys. Res.*, *107*(C9), 3128, doi:10.1029/2001JC000983.

Jessup, A. T., and V. Hesany (1996), Modulation of ocean skin by swell waves, *J. Geophys. Res.*, *101*, 6501–6511.

Jessup, A. T., R. A. Fogelberg, and P. Minnett (2002), Autonomous shipboard radiometer system for in situ validation of satellite SST, paper presented at Earth Observing Systems VII Conference, SPIE Int. Soc. Opt. Eng., Seattle, Wash.

Kearns, E. J., J. A. Hanafin, R. Evans, P. J. Minnett, and O. B. Brown (2000), An independent assessment of Pathfinder AVHRR sea surface temperature accuracy using the Marine-Atmosphere Emitted Radiance Interferometer, *Bull. Am. Meteorol. Soc.*, *81*, 1525–1536.

Liss, P. S., and L. Merlivat (1986), Air-sea gas exchange rates: Introduction and synthesis, in *The Role of Air-sea Exchange in Geochemical Cycling*, edited by P. Buat-Ménard, pp. 113–127, D. Reidel, Norwell, Mass.

Mammen, T. V., and N. von Bosse (1990), STEP—A temperature profiler for measuring the oceanic thermal boundary layer at the ocean-air interface, *J. Atmos. Oceanic Technol.*, *7*, 312–322.

McGillis, W. R., J. B. Edson, J. E. Hare, and C. W. Fairall (2001), Direct covariance air-sea CO_2 fluxes, *J. Geophys. Res.*, *106*, 16,729–16,745.

McNeil, C. L., and L. Merlivat (1996), The warm oceanic surface layer: Implications for CO_2 fluxes and surface gas measurements, *Geophys. Res. Lett.*, *23*, 3575–3578.

Murphy, P. P., Y. Nojiri, Y. Fujinuma, C. S. Wong, J. Zeng, T. Kimoto, and H. Kimoto (2001), Measurements of surface seawater fCO_2 from volunteer commercial ships: Techniques and experiences from Skaugran, *J. Atmos. Oceanic Technol.*, *18*, 1719–1734.

Nightingale, P. D., G. Malin, C. S. Law, A. J. Watson, P. S. Liss, M. I. Liddicoat, J. Boutin, and R. C. Upstill-Goddard (2000), In situ evaluation of air-sea gas exchange parameterizations using novel conservative and volatile tracers, *Global Biogeochem. Cycles*, *14*, 373–387.

Ohlmann, J. C., and D. A. Siegel (2000), Ocean radiant heating: II. Parameterizing solar radiation transmission through the upper ocean, *J. Phys. Oceanogr.*, *30*, 1849–1865.

Paulson, C. A., and J. J. Simpson (1981), The temperature difference across the cool skin of the ocean, *J. Geophys. Res.*, *86*, 11,044–11,054.

Price, J. F., R. A. Weller, and R. Pinkel (1986), Diurnal cycling: Observations and models of the upper ocean response to diurnal heating, cooling, and wind mixing, *J. Geophys. Res.*, *91*, 8411–8427.

Robertson, J. E., and A. J. Watson (1992), Thermal skin affect of the surface ocean and its implication for CO_2 uptake, *Nature*, *358*, 738–740.

Sarmiento, J. L., and E. T. Sundquist (1992), Revised budget for the oceanic uptake of anthropogenic carbon dioxide, *Nature*, *356*, 589–593.

Schlüssel, P., W. J. Emery, H. Grassl, and T. Mammen (1990), On the bulk skin temperature difference and its impact on satellite remote sensing of sea surface temperature, *J. Geophys. Res.*, *95*, 13,341–13,356.

Soloviev, A. V., and P. Schlüssel (1996), Evolution of cool skin and direct air-sea gas transfer coefficient during daytime, *Boundary Layer Meteorol.*, *77*, 45–68.

Takahashi, T., J. Olafsson, J. G. Goddard, D. W. Chipman, and S. C. Sutherland (1993), Seasonal variations of CO_2 and nutrients in the high-latitude surface oceans: A comparative study, *Global Biogeochem. Cycles*, *7*, 843–878.

Takahashi, T., R. A. Feely, R. F. Weiss, R. Wanninkhof, D. W. Chipman, S. C. Sutherland, and T. T. Takahashi (1997), Global air-sea flux of CO_2: An estimate based on measurements of sea-air pCO_2 difference, *Proc. Natl. Acad. Sci. U. S. A.*, *94*, 8292–8299.

Tans, P. P., I. Y. Fung, and T. Takahashi (1990), Observational constraints on the global atmospheric CO_2 budget, *Science*, *247*, 1431–1438.

Van Scoy, K. A., K. P. Morris, J. E. Robertson, and A. J. Watson (1995), Thermal skin affect and the air-sea flux of carbon dioxide: A seasonal high-resolution estimate, *Global Biogeochem. Cycles*, *9*, 253–262.

Wanninkhof, R. (1992), Relationship between wind speed and gas exchange over the ocean, *J. Geophys. Res.*, *97*, 7373–7382.

Wanninkhof, R., and W. R. McGillis (1999), A cubic relationship between air-sea CO_2 exchange and wind speed, *Geophys. Res. Lett.*, *26*, 1889–1892.

Wanninkhof, R., and K. Thoning (1993), Measurement of fugacity of CO_2 in surface water using continuous and discrete sampling methods, *Mar. Chem.*, *44*, 189–204.

Ward, B., and P. J. Minnett (2002), An autonomous profiler for near surface temperature measurements, in *Gas Transfer at Water Surfaces*, *Geophys. Monogr. Ser.*, vol. 127, edited by M. Donelan et al., pp. 167–172, AGU, Washington D. C.

Ward, B., R. Wanninkhof, P. J. Minnett, and M. Head (2004), SkinDeEP: A profiling instrument for upper decameter sea surface measurements, *J. Atmos. Oceanic Technol.*, *21*, 207–222.

Weiss, R. F. (1974), Carbon dioxide in water and seawater: The solubility of a non-ideal gas, *Mar. Chem.*, *2*, 203–215.

Wick, G. A., W. J. Emery, L. H. Kantha, and P. Schlüssel (1996), The behavior of the bulk-skin sea surface temperature difference under varying wind speed and heat flux, *J. Phys. Oceanogr.*, *26*, 1969–1988.

Wong, C. S., Y.-H. Chan, and J. S. Page (1995), Geographical, seasonal and interannual variations of air-sea CO_2 exchange in the subtropical Pacific surface waters during 1983–1988, *Tellus, Ser. B*, *47*, 431–446.

M. D. DeGrandpre, Department of Chemistry, University of Montana, Missoula, MT 59812, USA. (mdegrand@selway.umt.edu)

J. B. Edson, W. R. McGillis, and B. Ward, Department of Applied Ocean Physics and Engineering, Woods Hole Oceanographic Institution, 98 Water Street, Woods Hole, MA 02543, USA. (jedson@whoi.edu; wmcgillis@whoi.edu; bward@whoi.edu)

J. E. Hare, Cooperative Institute for Research in Environmental Sciences, University of Colorado, 216 UCB, Boulder, CO 80309, USA. (jeff.hare@noaa.gov)

A. T. Jessup, Applied Physics Laboratory, University of Washington, 1013 NE 40th Street, Seattle, WA 98105-6698, USA. (jessup@apl.washington.edu)

R. Wanninkhof, Atlantic Oceanographic and Meteorological Laboratory, 4301 Rickenbacker Causeway, Miami, FL 33149, USA. (rik.wanninkhof@noaa.gov)